ELSEVIER

Contents lists available at ScienceDirect

Earth and Planetary Science Letters

www.elsevier.com/locate/epsl



XRF analysis of Laguna Pallcacocha sediments yields new insights into Holocene El Niño development



Samuel Z. Mark ^{a,*}, Mark B. Abbott ^a, Donald T. Rodbell ^b, Christopher M. Moy ^c

- ^a University of Pittsburgh, Department of Geology and Environmental Science, United States of America
- ^b Union College, Department of Geology, United States of America
- ^c University of Otago, Department of Geology, New Zealand

ARTICLE INFO

Article history: Received 18 March 2022 Received in revised form 31 May 2022 Accepted 5 June 2022 Available online xxxx Editor: Y. Asmerom

Keywords: Holocene ENSO XRF tropical Pacific flood history paleolimnology

ABSTRACT

The laminated sedimentary sequence of Ecuador's Laguna Pallcacocha is one of the most widely cited proxy records of Holocene El Niño Southern Oscillation (ENSO) variability. Previous efforts to reconstruct flood-driven laminae from Laguna Pallcacocha relied solely on sediment color, a useful but non-specific metric of flood events. We improved the chronology with ²¹⁰Pb and additional ¹⁴C dates over the past millennium, which allows for comparison of the sedimentary record with historically documented El Niño events. Additionally, we use elemental composition derived from X-ray Fluorescence (XRF) to reconstruct flood history at Pallcacocha. A principal component analysis (PCA) of the XRF dataset identifies minerogenic flood-driven clastic laminae. The first principal component (PC1) of the XRF data and red color intensity are positively correlated over the past 7.5 kyr, but the color record fails to capture high frequency variability that is preserved in the XRF dataset during the early Holocene (approximately 7.5-11 kyr BP). The new XRF dataset indicates moderate El Niño activity during the early Holocene, suppressed El Niño activity in the middle Holocene, and enhanced El Niño activity during the late Holocene. This pattern is relatively common among other ENSO records, and has been attributed to long-term changes in tropical insolation. Some intervals-most notably between 3-2 kyr BP and during the last millennium-deviate from expected trends if insolation was the sole forcing mechanism. Previously proposed mechanisms linking ENSO to latitudinal displacement of the ITCZ and ocean-atmospheric variabilities in other ocean basins appear to play an additional role in modulating Holocene ENSO development, as demonstrated by statistically significant correlations between the revised Laguna Pallcacocha flood history and proxy records from the Atlantic.

© 2022 Elsevier B.V. All rights reserved.

1. Introduction

Despite the significance of the El Niño Southern Oscillation (ENSO) to global climate and human society, its behavior over the course of the Holocene remains widely debated. Existing proxy records from lake sediments (Rodbell et al., 1999; Moy et al., 2002; Thompson et al., 2017; Zhang et al., 2014), foraminifera (Koutavas and Joanides, 2012), bivalve shells (Carré et al., 2014) and speleothems (Chen et al., 2016; Griffiths et al., 2020), as well as evidence from modeling experiments (e.g. Chen et al., 2019; Zheng et al., 2008) indicate reduced El Niño activity during the middle Holocene (7.5-4 kyr BP). However, other high-resolution proxy records from coral skeletons (Cobb et al., 2013; Emile-Geay et al., 2016) and molluscan assemblages (Emile-Geay et al., 2016)

highlight the pronounced variability of past ENSO changes. Further demonstrating the complexity of pre-instrumental ENSO variability, continuous, high resolution proxy records from tree-ring and speleothem records have yet to yield a conclusive picture of ENSO variability during the Little Ice Age (LIA, 1450-1850 AD) and Medieval Climate Anomaly (MCA, 900-1300 AD) (Henke et al., 2017). For instance, while some records indicate increased El Niño activity, or persistent El Niño-like conditions during the Medieval Climate Anomaly (MCA) (Tan et al., 2019), other records indicate the opposite pattern (Denniston et al., 2015). Reconciling these divergent conclusions is a crucial and necessary step for better understanding long-term forcing of ENSO variability.

Several studies have implicated insolation as a major driver of El Niño frequency. Modeling studies and observational data suggest an inverse relationship between seasonal temperature contrast and ENSO activity, as enhanced seasonality strengthens Pacific Walker Circulation, and suppresses the development of El Niño events (An and Choi, 2014; Zheng et al., 2008). While some proxy records

^{*} Corresponding author.

E-mail address: szm18@pitt.edu (S.Z. Mark).

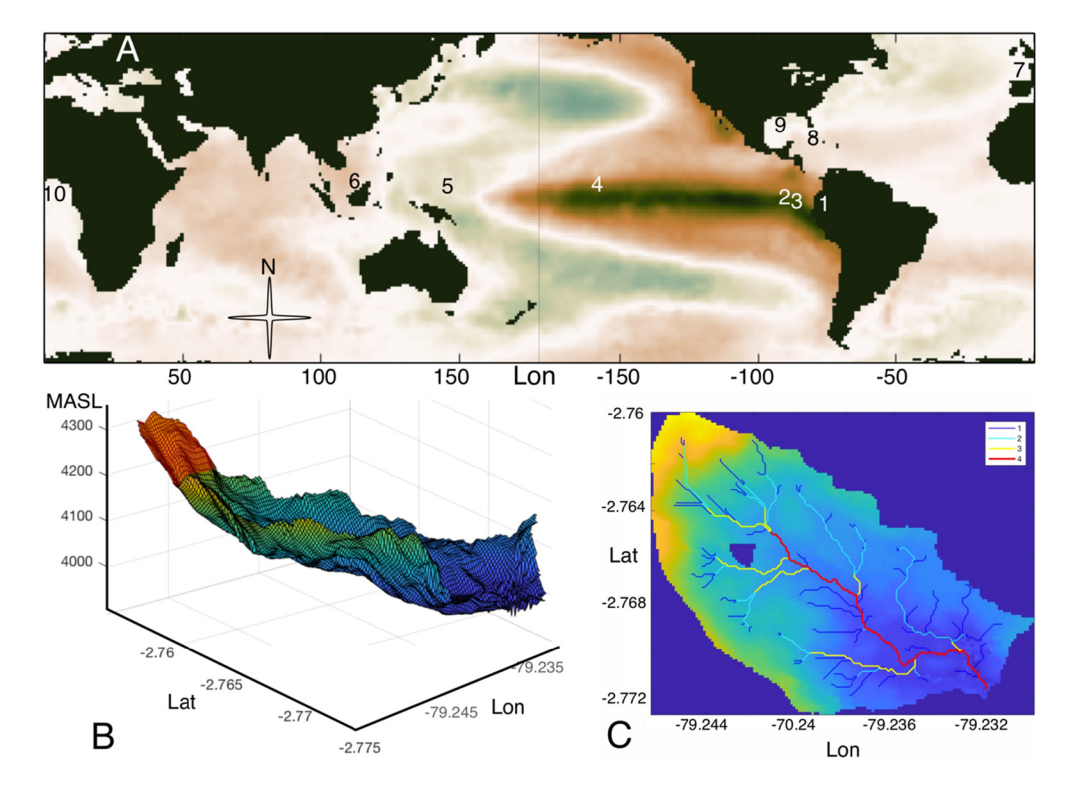


Fig. 1. First EOF of sea surface temperatures (SST), 60N to 60S. Location of ENSO-sensitive proxies discussed in text are designated as follows: (1) Laguna Pallcacocha (this study), (2) El Junco, Galapagos (Zhang et al., 2014), (3) Marine Core V21-30 (Koutavas and Joanides, 2012), (4) Northern Line Islands coral chronology (Grothe et al. 2020), (5) Indo-Pacific Warm Pool marine core compilation (Dang et al., 2020), and (6) Bukit Assam Cave, Borneo (Chen et al., 2016). Proxies sensitive to Atlantic phenomena are designated as (7) Kaite Cave, Spain (Domínguez-Villar et al., 2017), (8) Florida Straits marine core (Schmidt et al., 2012), (9) Gulf of Mexico marine core (Poore et al., 2003), and (10) Gulf of Guinea core GEO-B4509 (Collins et al., 2017). Plotting conducted using the Climate Data Toolbox for MATLAB (Greene et al., 2019) (B) 3D rendering of the Laguna Pallcacocha watershed. The transparent red outline at headwall shows the zone of loose, clastic sediment production. (C) Horton stream order map of the Laguna Pallcacocha watershed, showing the network of channels which connect the zone of clastic sediment production to the lake. Color of channel indicates Horton stream order. (For interpretation of the colors in the figure(s), the reader is referred to the web version of this article.)

have supported this mechanism (McGregor et al., 2013), a Pacificwide compilation of sub-annually resolved $\delta^{18}O_{aragonite}$ records dispute such a mechanism (Emile-Geay et al., 2016). Other studies have indicated that higher equatorial September (White et al., 2018: Dang et al., 2020) and June (Dang et al., 2020) insolation enhances the zonal tropical Pacific thermal gradient and suppresses the development of El Niño events via shoaling of the eastern Pacific thermocline. However, high-resolution proxy records from the core ENSO region (equatorial tropical Pacific) demonstrate the importance of centennial-scale shifts in ENSO variability which cannot be explained solely by changes in insolation (Cobb et al., 2013). Abrupt, stepwise southward shifts in the intertropical convergence zone (ITCZ) (Haug et al., 2001), explosive volcanism (Stevenson et al., 2016) and teleconnections to the Atlantic basin (Pausata et al., 2017; Levine et al., 2017) have all been proposed as additional drivers of ENSO variability.

The laminated sedimentary record of Laguna Pallcacocha, Cajas National Park, Ecuador, is unique among ENSO proxies in its temporal resolution and continuity (Rodbell et al., 1999; Moy et al., 2002). During an El Niño event, the waters of the tropical eastern Pacific experience anomalous warming and convection, generating intense cloudbursts at Laguna Pallcacocha (Fig. 1) (Kiefer and Karamperidou, 2019). The resultant floods carry eroded clastic sediments from the exposed ignimbrite headwalls of the catchment (Fig. 1B) into the lake via a single fourth-order stream (Fig. 1C), where these sediments are deposited as visibly identifiable, light colored, fine-grained (\sim 5 µm) clastic layers. The abundance of clastic laminae, captured by analysis of grayscale (Rodbell et al., 1999) and red color intensity (Moy et al., 2002) variations, has been interpreted to reflect the frequency of El Niño events over the past

11,000 years. The Pallcacocha sedimentary record derived from visible color metrics indicates suppressed El Niño activity during the early and middle Holocene, with the modern ENSO regime being established about 5 kyr BP and maximum El Niño frequency occurring approximately 1,200 yr BP (Moy et al., 2002; Rodbell et al., 1999).

Several studies have sought to re-evaluate the clastic alluviation signal preserved in Laguna Pallcacocha's sedimentary record using different approaches. Schneider et al. (2018) found no significant relationship between flood driven alluviation events and instrumental El Niño records. This study failed to find clastic laminae corresponding to the very strong 1982/83 and 1997/98 CE El Niño events in surface cores. However, the cores were collected after significant landscape disturbance in the watershed and repeated coring of the small deep basin of the lake. Additionally, using a network of meteorological stations located up to 50 km east of the Andean divide, Schneider et al. (2018) found no significant relationship between 24 and 36 hour precipitation maxima and El Niño conditions. The only station proximal (<5 km) to Pallcacocha, however, covers only 4 years (2012-2016 CE). More recent work, however, has concluded that alluviation at Laguna Pallcacocha is, in fact, closely tied to El Niño events when sea surface temperature (SST) warming is centered in the eastern Pacific and coastal South America (EP and COA events, respectively). During EP and COA events, westerly winds and cloudburst rainfall occur at Laguna Pallcacocha, but not at a nearby weather station several kilometers east of and more than 500 m lower than the lake (Hagemans et al., 2021). This is consistent with a meso-scale modeling experiment which suggests that EP and COA ENSO events drive intense hourly precipitation maxima, while having relatively little impact

on overall precipitation totals (Kiefer and Karamperidou, 2019). These convective cloudbursts are responsible for generating alluviation and clastic sedimentation in the Laguna Pallcacocha sedimentary record.

Additional work is needed on the Laguna Pallcacocha record to directly link watershed-scale erosion to climate, evaluate how the record may record newly recognized configurations of ENSO, and compare the clastic stratigraphy to the growing body of paleo-ENSO proxy records. The original work was done prior to advances in age modeling and suffers from limited chronological control over the past millennium. Additionally, the visible color stratigraphy may in part reflect a variety of environmental and ecological processes unrelated to rapid depositional events. High-resolution XRF-derived elemental content offers the advantage of directly linking sedimentary structures with erosion and deposition in the watershed. Few, if any, Holocene ENSO reconstructions have both the temporal resolution to record individual El Niño events and provide continuous coverage over the Holocene. Most modeling experiments only cover discrete, centennial-scale windows of climate variability, hindering an exploration of ENSO evolution and its relationship to external factors (Emile-Geay et al., 2016). As such, improving the temporal constraints and refining the interpretation of the Laguna Pallcacocha record is vital to the future of paleo-ENSO research.

Here, we address critical questions regarding the Pallcacocha record. We use surface cores recovered in 1993, 1998, 2014, 2017, and 2018 CE to examine the relationship between El Niño events, environmental change, and clastic sedimentation in the basin. By using ¹³⁷Cs and ²¹⁰Pb assays, we improved the chronology over the recent past, and can directly compare depositional events in the stratigraphy to instrumental and documentary records of warming in the eastern tropical Pacific. Third, and most significantly, we present a high-resolution record of XRF-derived elemental composition to directly link clastic debris flow events to sedimentation during the Holocene. The resultant flood chronology, interpreted as showing long-term changes in coastal and eastern Pacific El Niño events, sheds new light on the development of ENSO over the Holocene and can be used to investigate potential forcing mechanisms.

2. Methods

2.1. Core collection

Surface cores were collected using a 5.9 cm diameter polycarbonate tube and piston in 1999, 2017, and 2018 and transported intact to the laboratory using sodium polyacrylate to stabilize the surface (Fig. 2). A freeze core was collected in 2017 to ensure insitu preservation of sediment (Fig. 2). Full Holocene sections were recovered with a Livingstone corer in 1993 and 1999, however sediment-water interfaces were disturbed during these coring operations. All cores described here were collected from the deepest (~8 meter) basin identified by Rodbell et al. (1999).

2.2. Chronology

We constrained the ages of surface sediments using an unpublished ²¹⁰Pb chronology from the 1999 surface core and a ²¹⁰Pb chronology from a surface core collected in 2017, modeled using both a Constant Rate of Supply (CRS) and Constant Flux Constant Sedimentation (CFCS) model after eliminating clastic layers following the assumption that they were essentially instantaneous events (Arnaud et al., 2002) (Fig. S1). In addition, 5 radiocarbon dates were measured and combined with the original 14 radiocarbon dates from Rodbell et al. (1999). Two of them were measured

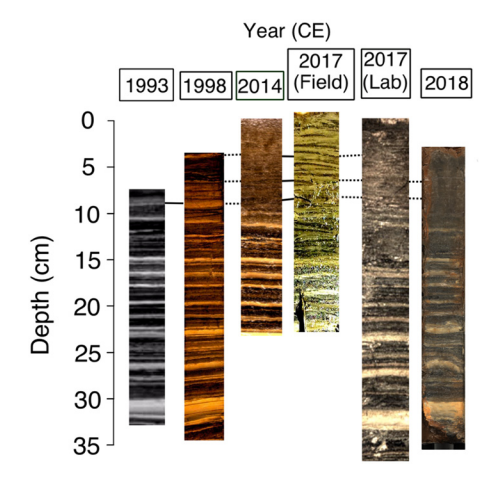


Fig. 2. Pallcacocha surface cores taken between 1993 and 2018 show common visual features beneath roughly 15 cm, but not necessarily at the core tops. Solid black lines indicate stratigraphic features which are reproduced, while dashed black lines indicate features which are not.

at the Penn State Radiocarbon Laboratory on a National Electrostatics Corporation 500 kV 1.5SDH-1 Compact Accelerator Mass Spectrometer and three were measured at the W.M Keck Carbon Cycle Accelerator Mass Spectrometer at the University of California Irvine on a similar system. All samples were prepared with a standard acid-base-acid method (Santos and Ormsby, 2013). A well-dated tephrochronology from the region provides additional chronological tie-points (Rodbell et al., 2002) and allows for depth adjustments to account for the amount the cores have shrunk over the past 20 years. A complete age-depth model, with age uncertainty, was developed using the Bchron software package (Parnell and Parnell, 2021) and the IntCal20 calibration curve (Hogg et al., 2020). The initial age model developed by Rodbell et al. (1999) and further advanced by Moy et al. (2002) uses a Constant Carbon Accumulation (CCA) model to account for rapid depositional events in the core. While the relatively short-lived depositional events surely alter instantaneous sedimentation rate, the sequence in its entirety displays a relatively constant sedimentation rate (Fig. S1), making age modeling techniques that account for rapid alluvial events unnecessary over the timescale of the full record.

2.3. X-ray fluorescence and sedimentology

In 2017 the Livingstone cores collected in 1999 were scanned with an ITRAX XRF Core scanner at the Large Lakes Observatory at the University of Minnesota Duluth, which provides elemental counts for most elements less than atomic number 93. The cores were scanned at 0.1 cm resolution with a 15 second dwell time. Total organic content (TOC) was measured by loss on ignition and converted to TOC via a transfer function (Rodbell et al., 1999).

3. Results

3.1. Laguna Pallcacocha XRF record

Al, Si, K, and Rb are all positively correlated with one another for the entirety of the record (Fig. 4). Higher counts are associated with the light-colored clastic laminae and the inorganic (glacial) silt at the base of the sequence. The ratio of incoherent to coherent scatter (inc/coh) is associated with organic matter in the core and is significantly anti-correlated with Al, Si, Rb, and Ti. Unlike other lithophilic elements commonly derived from the catchment (Davies et al., 2015), Ti is not substantially higher during the deglacial period. We performed a principal component anal-

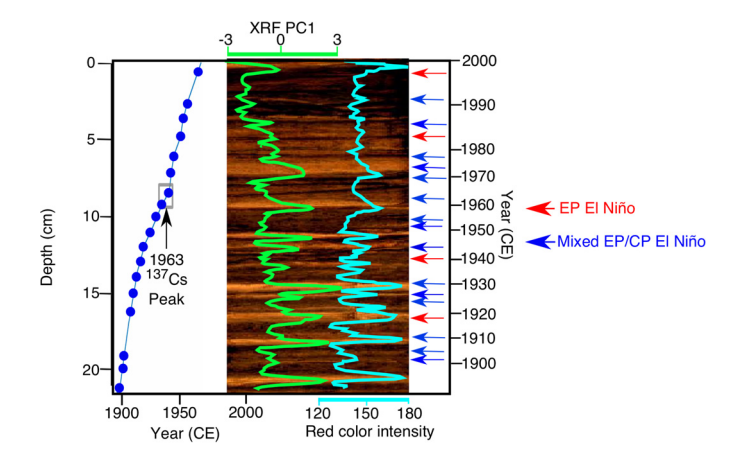


Fig. 3. 1999 surface core image with new 210Pb and 137Cs age model. Blue dots indicate depths at which assays were conducted. Grayscale (blue line) and XRF PC1 (green line) show close agreement with one another. Light colored clastic laminae, captured by both metrics, show close correlation with Eastern Pacific El Niño events, marked by red arrows and mixed EP/CP events by blue arrows, according to the classification scheme of Andreoli et al. (2017), which extends to CE 1902.

ysis on the variables mentioned above. The first principal component (PC1) of the XRF data (Fig. 4 B and C) is closely related to Al, Si, K, and Rb, consistent with the results of Schneider et al., 2018, and is interpreted as a proxy for alluvial deposits. The PC1 is the only significant component in the dataset, comprising 60% of the total variance. We interpret the PC1, and the elements positively correlated with it, as representing erosional input from clastic sediments in the catchment. PC1 is consistently higher prior to approximately 11.5 kyr BP, when sediments are characteristic of inorganic glacial till. The spacing of the high-frequency peaks, which we interpret as rapid alluviation events, represents the frequency of flooding over the course of the Holocene. In order to better visualize the frequency of flood events, peaks in the XRF PC1 were binned in 100 year intervals per the methodology of Moy et al. (2002) (Fig. 7A). Additionally, the return interval of flood events (i.e. the years between flood layers) were also calculated to emphasize higher-frequency variability (Fig. 8). Floods during the early Holocene tended to occur between roughly 8-12 times per century for an approximately 10-year return interval. During the middle Holocene, flood frequency decreased to approximately between 5-8 events per century (approximately 20 year return intervals). After approximately 4 kyr BP, flood frequency begins to increase, entering the modern ENSO frequency band (sub-decadal return interval, approximately 12-16 events per century) at about 2 kyr BP.

When both proxies are placed on the same (new) depth scale, the PC1 closely matches the variability in red color intensity values throughout the surface core (Fig. 3) and during the late to middle Holocene, but the two time series become dissimilar at greater depths (Figs. 4 and 5). Most notably, while the PC1 captures significant sub-decadal scale variability during the early Holocene, these variations in the red intensity data are either absent or the amplitude is significantly reduced (Fig. 5). The correlation between the PC1 and red color intensity for the period 0-7 kyr BP is 0.58 (p < .05). However, during the period 7-11 kyr BP, the correlation coefficient is reduced to 0.33 (p \ll .05). The cores have shrunk in the two decades between the initial collection and recent XRF analyses, and even millimeter-scale discrepancies in the depth scale can create destructive interference between the two time series, likely reducing correlations between the color record and XRF record. A cross-wavelet analysis between the red color intensity record and the XRF PC1 reveals the importance of using elemental data as opposed to sediment color (Fig. S3). From the beginning of the Holocene to roughly 10 kyr BP both time series show few significant spectral properties. Between 10 and

7 kyr BP, the XRF PC1 shows significant periodicities in the 8-32 year waveband, at lower frequencies than the modern ENSO waveband, while the red color intensity data shows no such periodicity. Both time series share a common significance at a 32-year waveband between 7 and 5 kyr BP. The updated age model indicates maximum flood event frequency in both the XRF and red color intensity record occurs between 900-1200 CE, during the MCA. The subsequent LIA (1450-1850 CE) shows fewer flooding events than the MCA, but still more frequent El Niño events than most of the Holocene.

Previous work has indicated that organic carbon in the sedimentary sequence is dominantly terrestrial in origin (Fig. S4, Rodbell et al., 1999). Both the proportion and the rate of organic carbon deposition is higher during the early Holocene (Fig. S5). Perhaps most importantly, negative excursions in organic carbon concentration, indicating rapid alluviation events, are substantially more organic carbon-rich during the early Holocene than during the middle Holocene (Fig. S5). Because organic carbon in the sediment is primarily terrestrial, the increased proportion of carbon in the early Holocene is consistent with enhanced erosion of organic material diluting inorganic clastic sediment during rapid alluvial events. This dilution would prevent alluvial deposits from being identified in the red color intensity and grayscale datasets, and prevent a high-frequency signal from registering during the early Holocene.

3.2. Recent sedimentation at Laguna Pallcacocha and surroundings

Recent landscape disturbance and repeated coring within the small lake basin preclude the correlation of the uppermost Pallcacocha stratigraphy to instrumental climate records after 1999. While surface cores taken over the past 25 years are consistently reproducible below 15 cm, clastic layers above this boundary are not common to all cores (Fig. 2). A core taken in 1999, shortly after the very strong 1997/1998 EP El Niño shows a clear clastic layer at the top (Figs. 2 and 3). However, the surface core presented in Schneider et al. taken in 2014 does not show this flood laminae, as well as several preceding layers (Fig. 2). Three potentially overlapping mechanisms can explain these differences. (1) Kees Noreen (Utrecht University, written communication 2020) documents a tenfold increase in the presence of the eutrophic indicator diatom species discostella stelligera (Bush et al., 2017) beginning in 1994. This shift occurs concurrently with the 1994 paving of Highway E-582, the only land route connecting the major cities of Guayaquil and Cuenca, which runs through Cajas National Park and within 2 km of Laguna Pallcacocha. This has drastically enhanced vehicle traffic through the park, particularly over the past decade (Bandowe et al., 2018). Productivity has long been shown to influence sedimentary color (Hayes and Anthony, 1958), and the high flux of aquatic organic matter to the lakebed would likely dilute the clastic signal and may "mask" visually identifiable clastic layers. This road construction, as well as the observed proliferation of foot and mule paths connecting communities north of the Pallcacocha catchment to the highway, have produced documented impacts on local ecosystems (Astudillo et al., 2014). However, potential eutrophication and productivity proxies (Si/Ti and Mn/Fe ratios) do not indicate that changing trophic conditions have drastically altered the top of the sedimentary record. Oxidation reactions which mask visually identifiable layers after core collection may play a significant role in changing the color of core tops. A field photograph of the 2017 freeze core shows visible stratigraphy which is absent in subsequent laboratory photographs (Fig. 2), consistent with this suggestion. (2) It is possible that the repeated coring of the Pallcacocha basin (more than a dozen cores have

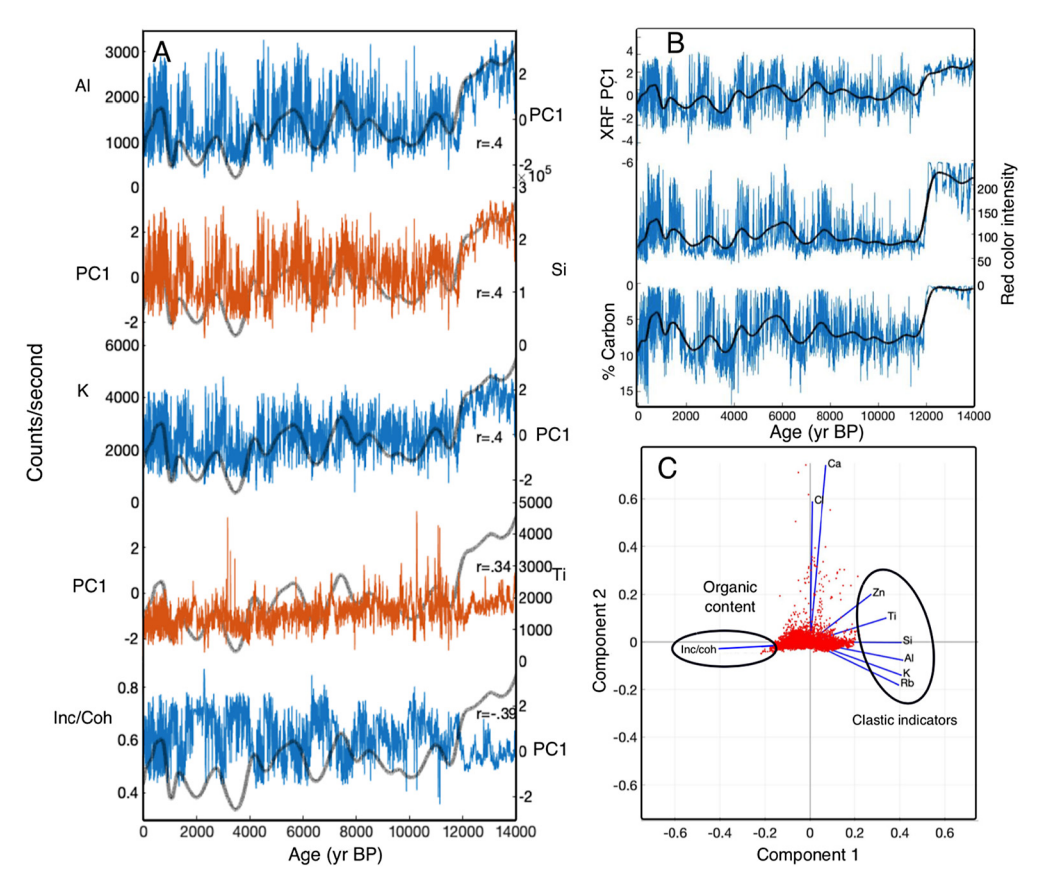


Fig. 4. (A) XRF-derived element counts from Laguna Pallcacocha, 100 point smoothing filter of the XRF PC1 is shown as transparent gray line. R values indicate correlation of each element with the PC1. (B) XRF PC1, organic carbon content, and red color intensity from Laguna Pallcacocha with 100-point smoothing filters (black lines). (C) Biplot of major elements from XRF Principal Component Analysis.

been extracted from a depocenter of roughly 1000 m²) may have created an uneven and artificially mixed surface sediment layer. The 2014 cores collected by Schneider et al. may have been taken from an area of the deep basin which has been disrupted over the past 20 years of research through repeated coring and anchoring efforts. Indeed, cores collected in 1993 and 1998 show several clear clastic layers which cannot be reproduced in all subsequent cores (Fig. 2). (3) Lastly, Hagemans et al. (2021) show recent (post 1998) debris flow events resulted in a channel avulsion which redirected the primary pathway for coarse sediment to be deposited away from the previous lake depocenter. This recent reworking of channel networks may confound the detection of modern depositional events. The size of the alluvial fan, and lack of geomorphic evidence for additional prominent channels in the watershed (Fig. 1C) indicate that alternative pathways of sedimentation have been minimal over the course of the Holocene. In sum, the combination of recent catchment alterations, sediment disturbance and changes in trophic status require that we limit quantitative correlations to historical and instrumental records of ENSO prior to 1999.

The addition of ²¹⁰Pb assays and ¹⁴C dates to the surface sediment core collected in 1999 substantially decreases age uncertainty over the past millennium, allowing for comparison with instrumental and historical evidence of El Niño events since 1550 CE (Fig. 3, Fig. 5). Between 1550 and 1900 CE, the period covered by several documentary reconstructions of El Niño events (Quinn et al., 1987; Garcia-Herrera et al., 2008), the Laguna Pallcacocha record documents 45 distinct flood laminae, one more than the number of El Niño events documented by Garcia-Herrera et al. (2008), when multi-year events are counted as a single El Niño

(Fig. 5). This is justified because multi-year events are likely indistinguishable from one flood deposit given the sub-millimeter scale of non-clastic sedimentation that would occur between floods. The documentary evidence provided by Garcia-Herrera et al. (2008) is the most reliable source to compare to recent sedimentation at Pallcacocha because of their shared sensitivity to coastal and eastern Pacific ENSO events. The Garcia-Herrera et al. (2008) chronology incorporates primary source evidence from the Spanish colonial administration in the city of Trujillo in northern Peru which is arid during non-El Niño years and receives precipitation in years with COA and EP El Niño events. The shared sensitivity to COA and EP events is reflected in the strong visual match between documented El Niño's and peaks in the XRF PC1 (Fig. 5A). While age uncertainty precludes the attribution of individual flood laminae to a specific year, the cumulative number of El Niño's recorded by Pallcacocha and the Garcia-Herrera et al. (2008) chronology between 1550 and 1990 CE is very similar (Fig. 5B). The period when the two cumulative event distributions diverge occur between the thickest clastic deposits over this period. Because these deposits occur approximately instantaneously, they distort the age model on interannual timescales (Moy et al., 2002). While the subtraction of clastic layers is justified over the ²¹⁰Pb chronology due to the high number of dates, further manual adjustment of the age model on interannual timescales is not justified. Despite these challenges, the remarkable consistency between documentary evidence and clastic sedimentation supports the notion of EP and COA El Niño events driving clastic sedimentation at Laguna Pallcacocha.

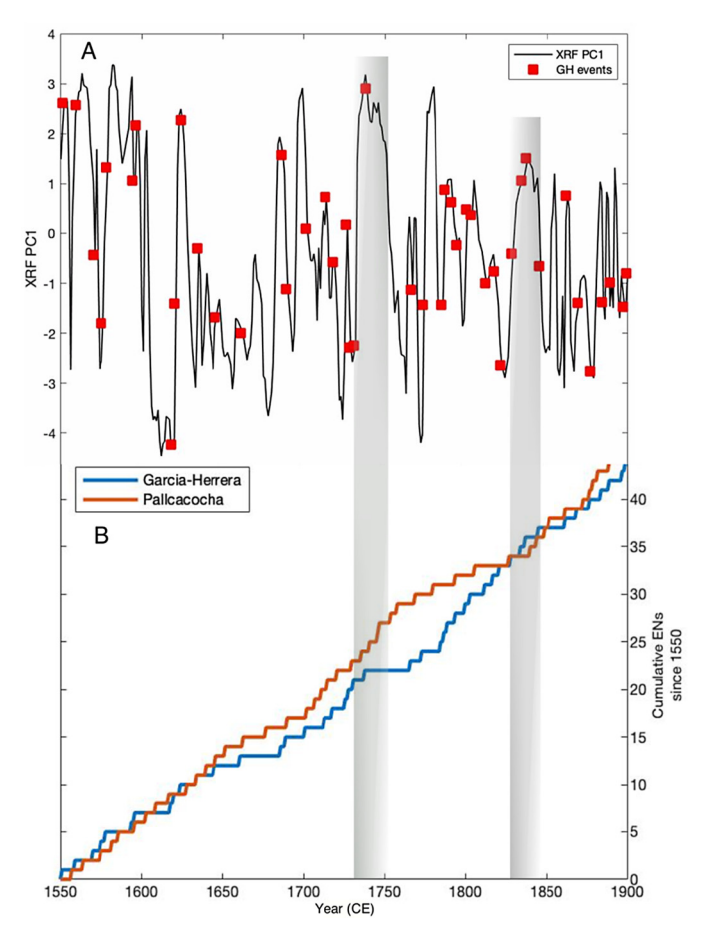


Fig. 5. (A) XRF PC1 (black line) and documentary evidence of El Niño events from primary documentary evidence detailed in Garcia-Herrera et al. (2008) (red squares). Peaks in XRF PC1 indicate clastic layers. While age uncertainty precludes absolute identification of the years in which clastic layers were deposited, the number of El Niño's (when counting events in concurrent years as a single event-see text) is almost identical (44 in the documentary evidence, 45 in the sedimentary record). (B) The cumulative number of El Niño events documented by Laguna Pallcacocha (red line) and the Garcia-Herrera et al. El Niño chronology (blue line) between 1550 and 1900 CE, the period covered by both records. Transparent gray boxes show thick layers of rapidly deposited clastic alluviation which occur coevally with divergence between the Laguna Pallcacocha and Garcia-Herrera event chronologies.

4. Discussion

4.1. The relationship between geochemical data, sediment color, and landscape change

Rapid alluviation events in the Laguna Pallcacocha sedimentary record are well represented by the first principal component (PC1) of the XRF data. Peaks in the PC1 represent abrupt deposition of clastic material resulting from El Niño-driven convective storm bursts consistent with the interpretations of Rodbell et al. (1999), Moy et al. (2002), and Hagemans et al. (2021) (Fig. 3). Measurements of Al, Si, K, and Rb in counts per second (cps) are all closely correlated with the XRF PC1 and are commonly used to identify clastic flood deposits in lacustrine settings (e.g. Berntsson et al., 2014). Additionally, each of these elements is significantly anti-correlated with Inc/Coh scatter, a commonly used proxy for organic content, as Carbon is too light to be detected by traditional scanning XRF techniques. Examination of the surface cores show that the visibly identifiable, fining upward sequences attributed to deposition by hyperpycnal flows by Rodbell et al. (1999) also appear as peaks in the PC1 (Fig. 3). Individual element counts each contain specific drawbacks, making the use of techniques like PCA preferable. While silica is an important component of the underlying ignimbrite bedrock, as evidenced by its elevated levels in glacial sediments, it can also reflect diatom frustule production (Peinerud, 2000). Titanium is an often-reliable indicator of terrestrial input (e.g., Haug et al., 2001), but it is also associated with larger grain size minerals of high specific gravity (Brown, 2015). This may explain why it is less abundant than the other detrital elements during the late glacial period, when sedimentation was primarily fine-grained glacial flour (Fig. S2). Catchment glaciers had completely melted by 12 kyr BP (Rodbell et al., 2008) making flood-driven alluviation the major delivery mechanism for clastic material through the Holocene. The use of PCA overcomes the limitations described above, and the linear combination of variables represented by the PC1 is a more reliable indicator of flood frequency from Laguna Pallcacocha than any single element.

Why, then, is color reliable indicator of clastic deposition during the middle and late Holocene, but not during the early Holocene? Unlike elemental composition, which is a direct function of mineralogy, color is influenced by a variety of environmental and limnological processes. Laminae discernable by color differences may have been formed less frequently during the deglacial period and early Holocene because of limited landscape stability. At present, high-altitude páramo ecosystems dominate the highlands of Cajas National Park, increasing soil carbon stocks and soil stability, even in steep watersheds (Minaya et al., 2016). Pollen records from the region indicate that these ecosystems have changed markedly over the course of the Holocene (Hansen et al., 2003). The transition to a páramo ecosystem resembling the modern environment occurred at 7,500 yr BP, coincident with the alignment between the XRF and color records. The early Holocene in Cajas National Park was marked by the presence of a dry season and increased biomass burning based on analyses of pollen and charcoal (Hansen et al., 2003). This pattern is reproduced at Laguna Llavillucu, a lower elevation site (3115 m a.s.l.) several kilometers east of Pallcacocha (Nascimento et al., 2020). The transition from a deglacial landscape to one dominated by páramo vegetation increased the stability of the watershed and hence the amount of erosion. Prior to the establishment of páramo vegetation at Laguna Pallcacocha, flood deposits contained higher proportions of terrestrial organic matter than during the middle and late Holocene when deep rooted tussock grasses protected soil from erosion (Fig. S4). Carbon isotopes and elevated TOC/TN ratios of organic matter indicate a predominantly terrestrial source. Generally elevated carbon isotope values during the early Holocene indicates a greater proportion of C4 to C3 land plants, a common phenomenon in postglacial Andean páramo ecosystems (Boom et al., 2001) (Fig. S4). Additionally, the transport of loose clastic material from the headwall where it is produced into the lake requires a network of channels and a prograding delta fan that developed over time. Mechanical abrasion continues to carve existing channels (Whipple et al., 2000), creating stream networks of sufficient competence and capacity to transport enough clastic material to register as visual laminae. Temporary sediment storage sites exist further upslope, forming much of the existing delta fan (Hagemans et al., 2021). While abrupt clastic sedimentation is still apparent in scanning XRF data, early Holocene flood deposits are less readily identifiable by red color intensity due to terrestrial ecosystem changes and landscape development.

4.2. Holocene history of El Niño preserved in Laguna Pallcacocha sediments

Changing orbital configurations have long been invoked to explain the apparent suppression of El Niño events in the early and (particularly) middle Holocene (Chen et al., 2019), a pattern broadly supported by the new XRF data from Pallcacocha. White et

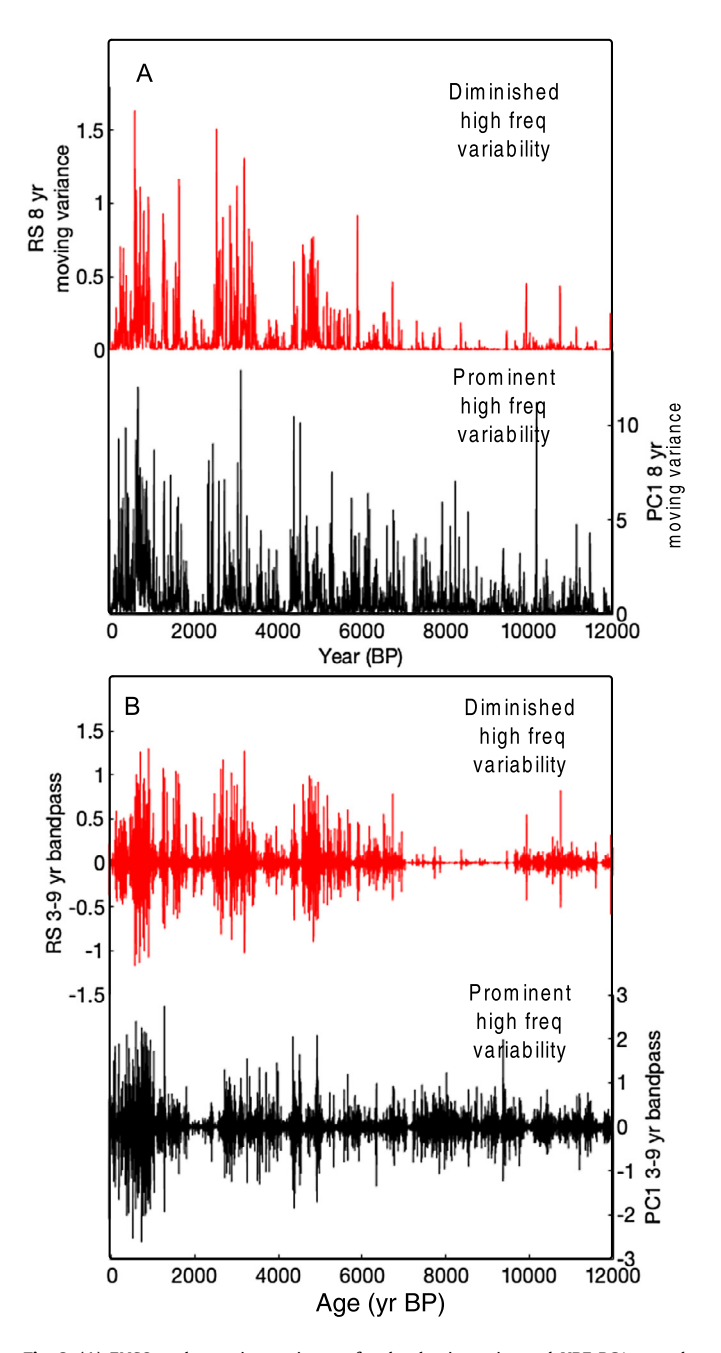


Fig. 6. (A) ENSO-scale moving variance of red color intensity and XRF PC1 records and (B) 3-9 year bandpass filter of red color intensity and PC1 from 0-12 kyr BP. Gray boxes indicate early Holocene period where high-frequency variability is muted in the color record but apparent in XRF PC1.

al. (2018) call attention to the role of enhanced equatorial June insolation in decreasing the depth of the eastern Pacific thermocline in the early and middle Holocene, dampening the upwelling feedback and hindering the formation of El Niño events. A compilation of marine sedimentary records from the Indo-Pacific Warm Pool (IPWP) highlights two significant orbital factors which limited El Niño activity by shoaling the thermocline and intensifying Walker Circulation prior to 4 kyr BP (Dang et al., 2020). The early Holocene thermocline warming is thought to be driven by June equatorial insolation maxima while the middle Holocene was driven by equatorial Oct-Dec insolation maxima (Dang et al., 2020), which inhibited the formation of El Niño events during their growth phase (Chen et al., 2016). Insolation driven seasonal contrast also peaks during the early Holocene, and has been suggested to hinder El Niño de-

velopment by exaggerating the zonal tropical Pacific temperature gradient, thereby accelerating Walker Circulation (McGregor et al., 2014). The new Laguna Pallcacocha XRF record, and others from the tropical Pacific (Fig. 6), indicate reductions in El Niño activity that are consistent with each mechanism described, suggesting that multiple orbital factors have been crucial to the development of the ENSO over the Holocene.

4.3. The role of volcanism, the ITCZ and other ocean basins in ENSO variability

While Holocene-scale trends in the Pallcacocha sedimentary record may relate to insolation forcing, robust centennial-decadal scale variability noted by other studies (Cobb et al., 2013; Emile-Geav et al., 2016) precludes the attribution of ENSO shifts to insolation alone. Several periods in particular show trends that cannot be clearly explained by orbital forcing. The Laguna Pallcacocha record, along with others (Fig. 7B, D), document a decrease in El Niño frequency between 3 and 2 kyr BP, a period which would have experienced enhanced El Niño activity if insolation alone were responsible for forcing long-term changes in the ENSO. The last millennium, a period covered by a multitude of highly-resolved, well-calibrated ENSO proxies remains uncertain and contested (Henke et al., 2017), with changing orbital configurations insufficient to explain the variability apparent in the proxy records. The Laguna Pallcacocha record indicates a higher frequency of El Niño events during the MCA than during the LIA, a pattern repeated by some other proxy records (Hereid et al., 2013). The influence of volcanic aerosol injection, as occurred after the Samalas eruption of the 1250's AD, has been widely investigated and debated (Dee et al., 2020; Stevenson et al., 2016). Recent work has shown that explosive volcanism may induce pronounced multi-decadal Pacific variability, which may in turn modulate the frequency of El Niño events (Mann et al., 2021; Sun et al., 2022).

Changes in the meridional extent of the ITCZ and its relationship to the ENSO, have also been the subject of considerable debate over the Holocene (Asmerom et al., 2020; Haug et al., 2001). The ENSO and the ITCZ are known to be closely related on interannual timescales. Northward displacement of the ITCZ, driven by northern hemisphere warming relative to the Southern Hemisphere, drives strong trade winds at the equator, enhancing upwelling and suppressing the development of El Niño events (Koutavas and Lynch-Stieglitz, 2004). Conversely, over the course of the instrumental record, El Niño events are associated with southward ITCZ displacements of up to 5 degrees (Schneider et al., 2014). Insolation is thought to drive latitudinal displacement of the ITCZ on a precessional timescale, with the ITCZ moving further south over the course of the Holocene in response to decreasing boreal summer insolation (Haug et al., 2001). This southward shift has also been invoked to explain a gradual strengthening of the South American Seasonal Monsoon (SASM) over the Holocene (Bird et al., 2011; Kanner et al., 2013). On shorter timescales, several proxies sensitive to Atlantic-derived SASM precipitation activity indicate abrupt drying after about 2 kyr BP (Schittek et al., 2015; Kanner et al., 2013) roughly coincident with an abrupt increase in El Niño events at Laguna Pallcacocha.

Many tropical proxy records from both hemispheres indicate a more northerly ITCZ location during the MCA, consistent with the proposed mechanism of northern hemisphere heating (cooling) driving latitudinal displacement of the ITCZ to the north (south) (Higley et al., 2018). However, there exists continued debate regarding whether this pattern is indicative of simple ITCZ displacement or ITCZ expansion and contraction (Lechleitner et al., 2017). Asmerom et al. (2020) use a highly resolved speleothem record from central Mexico to show that regions at the margins of the ITCZ belt in both hemispheres experience simultaneous drying and

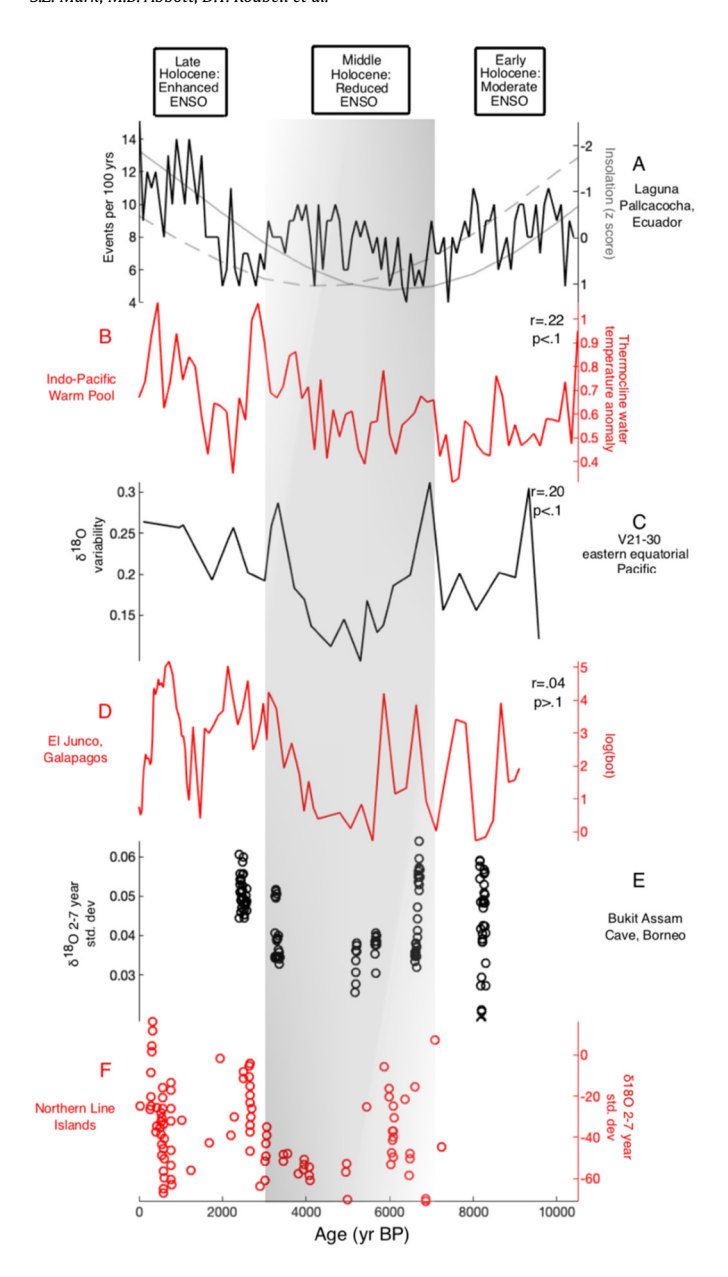


Fig. 7. Compilation of tropical Pacific ENSO records from 10,500 BP to present. Records indicate moderate ENSO activity in the early Holocene, reduced ENSO activity in the middle Holocene and enhanced ENSO during the late Holocene. Transparent gray box indicates middle Holocene period when continuous (A-D) and discontinuous (E and F) proxies indicate reduced ENSO variability. (A) El Niño events per 100 years from Laguna Pallcacocha (this study). Dashed gray line indicates equatorial Oct-Dec and solid gray line indicates equatorial seasonal insolation contrast (Mar-May vs. Oct-Dec). (B). Indo-Pacific Warm Pool thermocline water temperature anomaly (Dang et al., 2020) (C) δ18O variability, IODP drill site V21-30 (Koutavas and Joanides, 2011) (D) Concentration of *b. braunii*, El Junco Lake, Galapagos (Zhang et al., 2014) (E) 2-7 year bandpass filter δ18O, Bukit Assam Cave, Borneo speleothem (Chen et al., 2016) (F) (2-7 year bandpass filter δ18O concentrations from Northern Line Islands corals (Grothe et al., 2020). For continuous proxy records (B-D), r and p values between A and each panel are shown in the top right.

wetting during the MCA and LIA, respectively. A wavelet analysis of the speleothem record indicates that the annual migration of the ITCZ to its modern extent occurs at 1400 CE (550 yr BP) (Asmerom et al., 2020). Four runoff-driven lacustrine reconstructions of the ENSO from the eastern and western tropical Pacific record an abrupt transition from more active to less active ENSO conditions at approximately this time (Rodysill et al., 2019). Crucially, the Lake Lading, Indonesia, sedimentary record records La Niña, rather than El Niño, driven runoff and also indicates greater

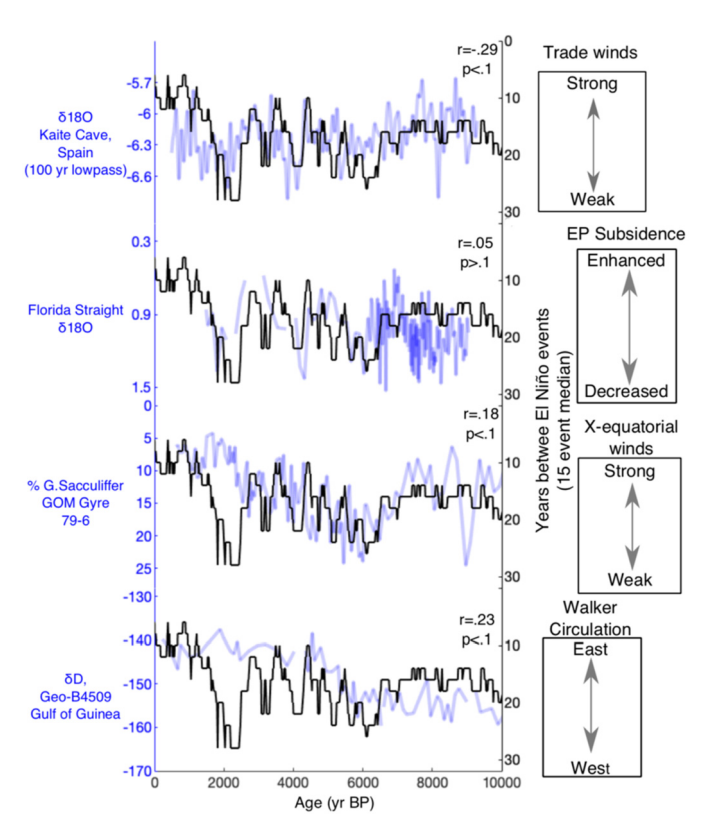


Fig. 8. Return interval of El Niño events (15 event rolling median, in black) at Laguna Pallcacocha and various proxy records from the Atlantic basin. Boxes on right indicate proposed interpretation of published proxy, while boxes on left offer potential explanations for how they influence the tropical Pacific. (A) Kaite Cave, Spain speleothem δ180 record (Domínguez-Villar et al., 2017). Degrees of freedom adjusted to account for lowpass filtering of original record when calculating p value. Potential relationship to ENSO described by Levine et al., 2017 (B) Florida Strait foraminiferal δ180 record. Relationship to ENSO described by McGregor et al. (2014) (C) % *G. sacculiffer* from Gyre 97-6 PC 20 (Poore et al., 2003). Potential relationship to ENSO described by Hu and Fedorov, 2018. (D) West African Monsoon reconstruction using hydrogen isotopes from Gulf of Guinea (Collins et al., 2017). Potential relationship to ENSO described by Pausata et al. (2017).

erosion during the MCA (Rodysill et al., 2019). The Laguna Pallcacocha and Lake Lading records dispute the characterization of the MCA and LIA as defined by persistently El Niño/La Niña like conditions. Instead, it appears the tropical Pacific during the MCA may have been defined by an ENSO system which oscillated on a shorter wavelength than during the LIA. However, discontinuous and lower-resolution proxy records from the last millennium show greater ENSO amplitude during the LIA than during the MCA (Rustic et al., 2015). A comparative absence of external forcing during the MCA may have led to stable conditions in ocean-atmospheric modes such as the ENSO (Bradley et al., 2016). This is reflected by the relatively frequent and consistent clastic depositional events at Laguna Pallcacocha. The tropical Pacific during the LIA may have been defined by stronger decadal and weaker interannual variability during the LIA (Wise and Dannenberg, 2014; D'Arrigo et al., 2001) which is reflected by relatively less frequent and consistent clastic layers in Laguna Pallcacocha.

A growing body of model (Levine et al., 2017) and proxy (Domínguez-Villar et al., 2017) studies have explored the relationship between the tropical Pacific and Atlantic Multidecadal Oscillation (AMO). Despite the complexities that are apparent in deciphering Pacific-Atlantic interactions, even during the modern era, the revised Pallcacocha record shows compelling similarities with proxy records from the Atlantic region (Fig. 8). Previous paleoclimate studies have found robust, significant correlations between Pallcacocha and proxies from the Atlantic (Domínguez-Villar et al.,

2017), linking a speleothem δ^{18} O record from Kaite Cave, Spain to the AMO, which in turn influences trade wind strength via the atmospheric bridge (Fig. 8A) (Levine et al., 2017). The temperature of the tropical North Atlantic, also influenced by the AMO has been shown to alter the location of the descending branch of Pacific Walker Circulation. Warming of the Florida Straits (Schmidt et al., 2012) is associated with decreased El Niño related flooding at Laguna Pallcacocha, consistent with a warmer tropical North Atlantic driving increased subsidence in the central and eastern tropical Pacific (Fig. 8B) (McGregor et al., 2014). The apparent reduction in El Niño frequency between 3 and 2 kyr BP occurs coevally with abrupt changes in the Kaite Cave and Florida Strait δ^{18} O records. While ENSO variability clearly responds to numerous forcing mechanisms, the congruencies linking the tropical Pacific and Atlantic variability warrant further investigation.

Proximal records interpreted as being sensitive to centennial scale shifts in the ITCZ (Poore et al., 2003) are consistent with changes in the frequency of flooding at Laguna Pallcacocha (Fig. 8C). Northward shifts of the tropical North Atlantic ITCZ have been shown in modeling studies to increase the strength of cross equatorial winds and induce a La Niña-like mean state in the tropical Pacific (Hu and Fedorov, 2018). Additionally, the strength of the West African Monsoon and the aridification of the Sahara have been shown to be crucial components in increased El Niño frequency during the late Holocene by shifting Pacific Walker Circulation westward causing La Niña like conditions (Pausata et al., 2017). Increasing El Niño event frequency over the middle and late Holocene occur contemporaneously with a weakening of the West African Monsoon, supporting this mechanism (Fig. 8D) (Collins et al., 2017; Griffiths et al., 2020). The long-term congruencies of records from different ocean basins and the abundance of proposed mechanistic relationships between the Atlantic Ocean and the ENSO suggest the persistence of complex, possibly time-lagged, linkages between Pacific and Atlantic oceanic-atmospheric variability. The development of further well-dated, high-resolution proxy records of ocean-atmospheric variability in the Atlantic will be crucial to improving an understanding of the complex linkages that influence ENSO on multi-decadal timescales. Disentangling Atlantic influence on the tropical Pacific from internally generated variability and externally forced changes will be crucial to anticipating long-term modulation of the ENSO system under different climate regimes.

4.4. Spatial heterogeneity of ENSO events

Increasing attention has been paid to the spatial heterogeneity of ENSO events, or ENSO "flavors" (Ashok et al., 2007). The vast spatial scale associated with the ENSO makes a comprehensive understanding of the entire system from a single proxy archive unreasonable. For example, a recent modeling study has indicated that during El Niño events with warming centered in the central Pacific, Laguna Pallcacocha receives relatively moderate and yearround rainfall. When warming is centered in the eastern tropical Pacific, however, convective activity and precipitation is enhanced (Kiefer and Karamperidou, 2019). This suggests the Laguna Pallcacocha record should be relatively insensitive to central Pacific (CP) El Niño events. Surface sediments from Laguna Pallcacocha appear to show flood deposits coincident with both eastern Pacific El Niño events and "mixed" El Niño when both EP and CP flavors occur in the same event (Andreoli et al., 2017). This is not surprising given that intense rainfall at Laguna Pallcacocha requires SST warming and convection in the eastern tropical Pacific. Statistically significant relationships exist between the Laguna Pallcacocha flood history and records from both the central and western Pacific (Dang et al., 2020) and eastern Pacific (Koutavas and Joanides, 2012) (Fig. 6), indicates there is some degree of coherence between the many flavors of the ENSO over multi-millennial timescales. A newly developed network of coral records (Freund et al., 2019) shows that the ratio of CP to EP events has increased in recent decades, while EP events have become more intense. The development of a continuous Holocene chronology of EP El Niño events will be crucial to testing hypotheses regarding the relationship between different flavors of the ENSO under different background climate conditions.

5. Conclusions

The Laguna Pallcacocha sedimentary record has long been cited as a continuous, high-resolution proxy record of El Niño events during the Holocene. Additional age constraints over the past millennium confirmed the link between rapid clastic sedimentation and historically documented El Niño's. Scanning XRF analysis identified flood-driven clastic laminae, which are not captured by previous studies which relied on sediment color analyses, between 11 and 7.5 kyr BP. Clastic laminae deposited during the early Holocene are marked by higher proportions of organic carbon, and were deposited prior to the establishment of the modern páramo which may have prevented erosion of the unstable upper soil horizon. The revised, erosion-based record of alluvial events at Laguna Pallcacocha more closely matches an emerging consensus of the ENSO over the course of the Holocene: moderate El Niño frequency before 7.5 kyr BP, suppressed El Niño frequency between 7.5 kyr and 4 kyr BP, and more active El Niño conditions after 4 kyr. This pattern is broadly consistent with proposed insolation controls on the ENSO-specifically June and September insolation maxima, which have the effect of warming the western Pacific and accelerating Walker Circulation. However, reduced El Niño frequency between 3 and 2 kyr BP and persistent centennial-scale variability throughout must be explained by other mechanisms. El Niño event frequency peaks during the MCA and relatively fewer events during the subsequent LIA. Proxy records from both sides of the Pacific also suggest more frequent La Niña events during the MCA, suggesting the MCA featured higher frequently oscillations of the ENSO system, rather than persistently El Niño/La Niña like conditions. Consistencies between the Laguna Pallcacocha record and proxy records from the tropical to sub-tropical Atlantic, lacking significant interannual relationships with the ENSO, suggest that previously proposed mechanisms linking the Atlantic and Pacific Oceans have operated over the course of the Holocene, and may explain some of the centennial-scale variability seen in tropical Pacific proxy records. The continuous, high-resolution Laguna Pallcacocha record offers a unique dataset that can be used to test hypotheses regarding ocean-atmosphere dynamics over the Holocene.

CRediT authorship contribution statement

Samuel Z. Mark: Conceptualization, Formal analysis, Investigation, Methodology, Visualization, Writing – original draft. **Mark B. Abbott:** Conceptualization, Funding acquisition, Investigation, Methodology, Writing – review & editing. **Donald T. Rodbell:** Conceptualization, Funding acquisition, Investigation, Methodology, Writing – review & editing. **Christopher M. Moy:** Investigation, Methodology, Writing – review & editing.

Declaration of competing interest

The authors declare that they have no known competing financial interests or personal relationships that could have appeared to influence the work reported in this paper.

Acknowledgements

We would like to thank two anonymous reviewers whose input greatly improved the quality of this manuscript. This project was funded by the National Science Foundation (grant number #502227), the University of Pittsburgh Department of Geology and Environmental Science, the University of Pittsburgh Climate and Global Change Center, and the Union College Geology Department. This work was also made possible by the Continental Scientific Drilling (CSD) Facility X-ray Fluorescence Lab at the University of Minnesota Duluth's Large Lakes Observatory, funded by the National Science Foundation (grant #502227).

Appendix A. Supplementary material

Supplementary material related to this article can be found online at https://doi.org/10.1016/j.epsl.2022.117657.

References

- An, S.-I., Choi, J., 2014. Mid-Holocene tropical Pacific climate state, annual cycle, and ENSO in PMIP2 and PMIP3. Clim. Dyn. 43 (3–4), 957–970.
- Andreoli, R.V., et al., 2017. The influence of different El Niño types on the South American rainfall. Int. J. Climatol. 37 (3), 1374–1390.
- Arnaud, F., et al., 2002. Flood and earthquake disturbance of ²¹⁰Pb geochronology (Lake Anterne, NW Alps). Terra Nova 14 (4), 225–232.
- Ashok, K., et al., 2007. El Niño Modoki and its possible teleconnection. J. Geophys. Res., Oceans 112 (C11).
- Asmerom, Y., et al., 2020. Intertropical convergence zone variability in the Neotropics during the Common Era. Sci. Adv. 6 (7). https://doi.org/10.1126/sciadv.
- Astudillo, P.X., et al., 2014. The impact of roads on the avifauna of páramo grasslands in Caias National Park, Ecuador, Stud. Neotrop, Fauna Environ, 49 (3), 204–212.
- Bandowe, B.A.M., et al., 2018. A 150-year record of polycyclic aromatic compound (PAC) deposition from high Andean Cajas National Park, southern Ecuador. Sci. Total Environ. 621, 1652–1663.
- Berntsson, A., et al., 2014. Late-Holocene temperature and precipitation changes in Vindelfjällen, mid-western Swedish Lapland, inferred from chironomid and geochemical data. Holocene 24 (1), 78–92.
- Bird, B.W., et al., 2011. Holocene tropical South American hydroclimate revealed from a decadally resolved lake sediment δ180 record. Earth Planet. Sci. Lett. 310 (3–4), 192–202.
- Boom, A., et al., 2001. High altitude C4 grasslands in the northern Andes: relicts from glacial conditions? Rev. Palaeobot. Palynol. 115 (3-4), 147-160.
- Bradley, R.S., et al., 2016. The medieval quiet period. Holocene 26 (6), 990-993.
- Brown, E.T., 2015. Estimation of biogenic silica concentrations using scanning XRF: insights from studies of Lake Malawi sediments. In: Micro-XRF Studies of Sediment Cores. Springer, pp. 267–277.
- Bush, M.B., et al., 2017. Human disturbance amplifies Amazonian El Niño-Southern Oscillation signal. Glob. Change Biol. 23 (8), 3181-3192.
- Carré, M., et al., 2014. Holocene history of ENSO variance and asymmetry in the eastern tropical Pacific. Science 345 (6200), 1045–1048.
- Chen, L., et al., 2019. Towards understanding the suppressed ENSO activity during mid-Holocene in PMIP2 and PMIP3 simulations. Clim. Dyn. 53 (1), 1095–1110.
- Chen, S., et al., 2016. A high-resolution speleothem record of western equatorial Pacific rainfall: implications for Holocene ENSO evolution. Earth Planet. Sci. Lett. 442, 61–71.
- Cobb, K.M., et al., 2013. Highly variable El Niño-Southern oscillation throughout the Holocene. Science 339 (6115), 67-70.
- Collins, J.A., et al., 2017. Rapid termination of the African Humid Period triggered by northern high-latitude cooling. Nat. Commun. 8 (1), 1–11.
- D'Arrigo, R., et al., 2001. Tree-ring estimates of Pacific decadal climate variability. Clim. Dvn. 18 (3), 219–224.
- Dang, H., et al., 2020. Pacific warm pool subsurface heat sequestration modulated Walker circulation and ENSO activity during the Holocene. Sci. Adv. 6 (42), eabc0402.
- Davies, S.J., et al., 2015. Micro-XRF Core Scanning in Palaeolimnology: Recent Developments. Micro-XRF Studies of Sediment Cores, pp. 189–226.
- Dee, S.G., et al., 2020. No consistent ENSO response to volcanic forcing over the last millennium. Science 367 (6485), 1477–1481.
- Denniston, R.F., et al., 2015. Extreme rainfall activity in the Australian tropics reflects changes in the El Niño/Southern Oscillation over the last two millennia. Proc. Natl. Acad. Sci. USA 112 (15), 4576–4581.
- Domínguez-Villar, D., et al., 2017. The control of the tropical North Atlantic on Holocene millennial climate oscillations. Geology 45 (4), 303–306.
- Emile-Geay, J., et al., 2016. Links between tropical Pacific seasonal, interannual and orbital variability during the Holocene. Nat. Geosci. 9 (2), 168.

- Emile-Geay, J., Tingley, M., 2016. Inferring climate variability from nonlinear proxies: application to palaeo-ENSO studies. Clim. Past 12 (1), 31–50.
- Freund, M.B., et al., 2019. Higher frequency of Central Pacific El Niño events in recent decades relative to past centuries. Nat. Geosci. 12 (6), 450–455.
- Garcia-Herrera, R., et al., 2008. A chronology of El Niño events from primary documentary sources in northern Peru. J. Climate 21 (9), 1948–1962.
- Greene, C.A., et al., 2019. The climate data toolbox for MATLAB. Geochem. Geophys. Geosyst. 20 (7), 3774–3781.
- Griffiths, M.L., et al., 2020. End of Green Sahara amplified mid-to late Holocene megadroughts in mainland Southeast Asia. Nat. Commun. 11 (1), 1–12.
- Grinsted, A., et al., 2004. Application of the cross wavelet transform and wavelet coherence to geophysical time series. Nonlinear Process. Geophys. 11 (5/6), 561–566.
- Grothe, P.R., et al., 2020. Enhanced El Niño-Southern oscillation variability in recent decades. Geophys. Res. Lett. 47 (7), e2019GL083906.
- Hagemans, K., et al., 2021. Patterns of alluvial deposition in Andean lake consistent with ENSO trigger. Quat. Sci. Rev. 259, 106900.
- Hansen, B., et al., 2003. Late-glacial and Holocene vegetational history from two sites in the western Cordillera of southwestern Ecuador. Palaeogeogr. Palaeoclimatol. Palaeoecol. 194 (1–3), 79–108.
- Haug, G.H., et al., 2001. Southward migration of the intertropical convergence zone through the Holocene. Science 293 (5533), 1304–1308.
- Hayes, F., Anthony, E., 1958. Lake water and sediment: I. Characteristics and water chemistry of some Canadian East coast lakes 1. Limnol. Oceanogr. 3 (3), 299–307
- Henke, L.M., et al., 2017. Was the little ice age more or less El Niño-like than the medieval climate anomaly? Evidence from hydrological and temperature proxy data. Clim. Past 13, 267–301.
- Hereid, K.A., et al., 2013. Coral record of reduced El Niño activity in the early 15th to middle 17th centuries. Geology 41 (1), 51–54.
- Higley, M.C., et al., 2018. Last millennium meridional shifts in hydroclimate in the central tropical Pacific. Paleoceanogr. Paleoclimatol. 33 (4), 354–366.
- Hogg, A.G., et al., 2020. SHCal20 Southern Hemisphere calibration, 0–55,000 years cal BP. Radiocarbon 62 (4), 759–778.
- Hu, S., Fedorov, A.V., 2018. Cross-equatorial winds control El Niño diversity and change. Nat. Clim. Change 8 (9), 798–802.
- Kanner, L.C., et al., 2013. High-resolution variability of the South American summer monsoon over the last seven millennia: insights from a speleothem record from the central Peruvian Andes. Quat. Sci. Rev. 75, 1–10.
- Kiefer, J., Karamperidou, C., 2019. High-resolution modeling of ENSO-induced precipitation in the tropical Andes: implications for proxy interpretation. Paleoceanogr. Paleoclimatol. 34 (2), 217–236.
- Koutavas, A., Joanides, S., 2012. El Niño-Southern oscillation extrema in the Holocene and last glacial maximum. Paleoceanography 27 (4).
- Koutavas, A., Lynch-Stieglitz, J., 2004. Variability of the marine ITCZ over the eastern Pacific during the past 30,000 years. In: The Hadley Circulation: Present, Past and Future. Springer, pp. 347–369.
- Lechleitner, F.A., et al., 2017. Tropical rainfall over the last two millennia: evidence for a low-latitude hydrologic seesaw. Sci. Rep. 7 (1), 1–9.
- Levine, A.F., et al., 2017. The impact of the AMO on multidecadal ENSO variability. Geophys. Res. Lett. 44 (8), 3877–3886.
- Mann, M.E., et al., 2021. Multidecadal climate oscillations during the past millennium driven by volcanic forcing. Science 371 (6533), 1014–1019.
- McGregor, H., et al., 2013. A weak El Niño/Southern Oscillation with delayed seasonal growth around 4,300 years ago. Nat. Geosci. 6 (11), 949–953.
- McGregor, S., et al., 2014. Recent Walker circulation strengthening and Pacific cooling applified by Alaptic warning. Not. Clim. Change 4 (10), 888, 803
- ing amplified by Atlantic warming. Nat. Clim. Change 4 (10), 888–892. Minaya, V., et al., 2016. Simulating Gross primary production and stand hydrological processes of páramo grasslands in the Ecuadorian Andean Region using the
- BIOME-BGC model. Soil Sci. 181 (7), 335–346. Moy, C.M., et al., 2002. Variability of El Niño/Southern Oscillation activity at millen-
- nial timescales during the Holocene epoch. Nature 420 (6912), 162. Nascimento, M., et al., 2020. The adoption of agropastoralism and increased ENSO
- frequency in the Andes. Quat. Sci. Rev. 243, 106471.
- Parnell, A., Parnell, M.A., 2021. Package 'Bchron'.
- Pausata, F.S., et al., 2017. Greening of the Sahara suppressed ENSO activity during the mid-Holocene. Nat. Commun. 8 (1), 1–12.
- Peinerud, E.K., 2000. Interpretation of Si concentrations in lake sediments: three case studies. Environ. Geol. 40 (1–2), 64–72.
- Poore, R., et al., 2003. Millennial-to century-scale variability in Gulf of Mexico Holocene climate records. Paleoceanography 18 (2).
- Quinn, W.H., et al., 1987. El Niño occurrences over the past four and a half centuries. J. Geophys. Res., Oceans 92 (C13), 14449–14461.
- Rodbell, D.T., et al., 2002. A late Glacial–Holocene tephrochronology for glacial lakes in southern Ecuador. Quat. Res. 57 (3), 343–354. Rodbell, D.T., et al., 1999. An∼ 15,000-year record of El Niño-driven alluviation in
- southwestern Ecuador. Science 283 (5401), 516–520. Rodbell, D.T., et al., 2008. Clastic sediment flux to tropical Andean lakes: records of
- glaciation and soil erosion. Quat. Sci. Rev. 27 (15–16), 1612–1626.
- Rodysill, J.R., et al., 2019. La Niña-driven flooding in the Indo-Pacific warm pool during the past millennium. Quat. Sci. Rev. 225, 106020.

- Rustic, G.T., et al., 2015. Dynamical excitation of the tropical Pacific Ocean and ENSO variability by Little Ice Age cooling. Science 350 (6267), 1537–1541.
- Santos, G.M., Ormsby, K., 2013. Behavioral variability in ABA chemical pretreatment close to the ¹⁴C age limit. Radiocarbon 55 (2–3), 534–544.
- Schittek, K., et al., 2015. Holocene environmental changes in the highlands of the southern Peruvian Andes (14 S) and their impact on pre-Columbian cultures. Clim. Past 11 (1), 27–44.
- Schmidt, M.W., et al., 2012. Solar forcing of Florida Straits surface salinity during the early Holocene. Paleoceanography 27 (3).
- Schneider, T., et al., 2014. Migrations and dynamics of the intertropical convergence zone. Nature 513 (7516), 45–53.
- Schneider, T., et al., 2018. Paleo-ENSO revisited: Ecuadorian Lake Pallcacocha does not reveal a conclusive El Niño signal. Glob. Planet. Change 168, 54–66.
- Stevenson, S., et al., 2016. "El Niño like" hydroclimate responses to last millennium volcanic eruptions. J. Climate 29 (8), 2907–2921.
- Sun, W., et al., 2022. Pacific multidecadal (50–70 year) variability instigated by volcanic forcing during the Little Ice Age (1250–1850). Clim. Dyn., 1–14.

- Tan, L., et al., 2019. Rainfall variations in central Indo-Pacific over the past 2,700 y. Proc. Natl. Acad. Sci. USA 116 (35), 17201–17206.
- Thompson, D.M., et al., 2017. Tropical Pacific climate variability over the last 6000 years as recorded in Bainbridge Crater Lake, Galápagos. Paleoceanography 32 (8), 903–922.
- Whipple, K.X., et al., 2000. River incision into bedrock: mechanics and relative efficacy of plucking, abrasion, and cavitation. Geol. Soc. Am. Bull. 112 (3), 490–503.
- White, S.M., et al., 2018. Dampened El Niño in the early and mid-Holocene due to insolation-forced warming/deepening of the thermocline. Geophys. Res. Lett. 45 (1), 316–326.
- Wise, E.K., Dannenberg, M.P., 2014. Persistence of pressure patterns over North America and the North Pacific since AD 1500. Nat. Commun. 5 (1), 1–6.
- Zhang, Z., et al., 2014. El Niño evolution during the Holocene revealed by a biomarker rain gauge in the Galápagos Islands. Earth Planet. Sci. Lett. 404, 420–424
- Zheng, W., et al., 2008. ENSO at 6ka and 21ka from ocean-atmosphere coupled model simulations. Clim. Dyn. 30 (7-8), 745-762.